Minimal upstream open reading frame of Per2 mediates phase fitness of the circadian clock to day/night physiological body temperature rhythm

AUTHOR(S):

Miyake, Takahito; Inoue, Yuichi; Shao, Xinyan; Seta, Takehito; Aoki, Yuto; Nguyen Pham, Khanh Tien; Shichino, Yuichi; ... Okamura, Hitoshi; Iwasaki, Shintaro; Doi, Masao

CITATION:

Miyake, Takahito ...[et al]. Minimal upstream open reading frame of Per2 mediates phase fitness of the circadian clock to day/night physiological body temperature rhythm. Cell Reports 2023, 42(3): 112157.

ISSUE DATE:

2023-03-28

URL:

http://hdl.handle.net/2433/281515

Article

Cell Reports

Minimal upstream open reading frame of *Per2* mediates phase fitness of the circadian clock to day/night physiological body temperature rhythm

Graphical abstract

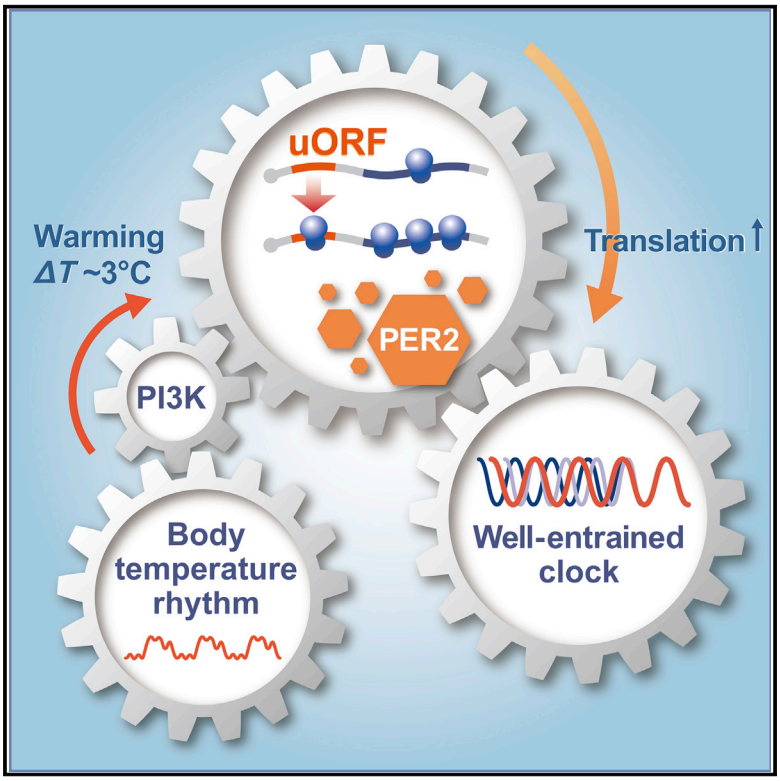

Authors

Takahito Miyake, Yuichi Inoue, Xinyan Shao, ..., Hitoshi Okamura, Shintaro Iwasaki, Masao Doi

Correspondence

doimasao@pharm.kyoto-u.ac.jp

In brief

Miyake et al. identify a minimal upstream open reading frame (uORF) in the 5′ UTR of the core clock gene *Per2*, which contributes to the circadian clock phase adaptation to day/night physiological body temperature cycles via the PI3K-mediated pathway. The *Per2* minimal uORF mediates maintenance of skin tissue homeostasis.

Highlights

- The circadian core clock gene *Per2* possesses a minimal uORF in the 5′ UTR
- The *Per2* minimal uORF binds ribosomes at increased temperature
- Circadian clock entrains to temperature via the *Per2* minimal uORF through PI3K
- The *Per2* minimal uORF modulates translation and mediates skin tissue maintenance

Miyake et al., 2023, Cell Reports *42*, 112157
March 28, 2023
https://doi.org/10.1016/j.celrep.2023.112157

CellPress

Cell Reports

CellPress OPEN ACCESS

Article

Minimal upstream open reading frame of *Per2* mediates phase fitness of the circadian clock to day/night physiological body temperature rhythm

Takahito Miyake,[1,8] Yuichi Inoue,[1,8] Xinyan Shao,[1] Takehito Seta,[1] Yuto Aoki,[1] Khanh Tien Nguyen Pham,[1] Yuichi Shichino,[2] Junko Sasaki,[3,4] Takehiko Sasaki,[3] Masahito Ikawa,[5] Yoshiaki Yamaguchi,[1] Hitoshi Okamura,[1,6] Shintaro Iwasaki,[2,7] and Masao Doi[1,9,*]

[1]Department of Systems Biology, Graduate School of Pharmaceutical Sciences, Kyoto University, Sakyō-ku, Kyoto 606-8501, Japan
[2]RNA Systems Biochemistry Laboratory, RIKEN Cluster for Pioneering Research, Wako, Saitama 351-0198, Japan
[3]Department of Biochemical Pathophysiology, Medical Research Institute, Tokyo Medical and Dental University, Bunkyō-ku, Tokyo 113-8510, Japan
[4]Department of Cellular and Molecular Medicine, Graduate School of Medical and Dental Sciences, Tokyo Medical and Dental University, Bunkyō-ku, Tokyo 113-8510, Japan
[5]Research Institute for Microbial Diseases, Osaka University, Suita, Osaka 565-0871, Japan
[6]Division of Physiology and Neurobiology, Graduate School of Medicine, Kyoto University, Sakyō-ku, Kyoto 606-8501, Japan
[7]Department of Computational Biology and Medical Sciences, Graduate School of Frontier Sciences, The University of Tokyo, Kashiwa, Chiba 277-8561, Japan
[8]These authors contributed equally
[9]Lead contact
*Correspondence: doimasao@pharm.kyoto-u.ac.jp
https://doi.org/10.1016/j.celrep.2023.112157

SUMMARY

Body temperature in homeothermic animals does not remain constant but displays a regular circadian fluctuation within a physiological range (e.g., 35°C–38.5°C in mice), constituting a fundamental systemic signal to harmonize circadian clock-regulated physiology. Here, we find the minimal upstream open reading frame (uORF) encoded by the 5′ UTR of the mammalian core clock gene *Per2* and reveal its role as a regulatory module for temperature-dependent circadian clock entrainment. A temperature shift within the physiological range does not affect transcription but instead increases translation of *Per2* through its minimal uORF. Genetic ablation of the *Per2* minimal uORF and inhibition of phosphoinositide-3-kinase, lying upstream of temperature-dependent Per2 protein synthesis, perturb the entrainment of cells to simulated body temperature cycles. At the organismal level, *Per2* minimal uORF mutant skin shows delayed wound healing, indicating that uORF-mediated Per2 modulation is crucial for optimal tissue homeostasis. Combined with transcriptional regulation, *Per2* minimal uORF-mediated translation may enhance the fitness of circadian physiology.

INTRODUCTION

Body temperature in homeothermic animals does not stay constant but displays a regular circadian fluctuation within a physiological range (e.g., 35°C–38.5°C in mice).[1–3] This rhythmic body temperature signal, generated by the master clock in the brain, provides a fundamental systemic signal to harmonize peripheral clocks throughout the body.[2,4,5] At the organismal level, this coherence between the master and peripheral tissue clocks confers an adaptive advantage, and its disruption has been suggested to decrease organismal fitness.[6,7] At the molecular level, the circadian rhythm-generating mechanism involves a set of clock genes, which control their own expression in a transcription-translation-based feedback loop.[5] Temperature affects this molecular timekeeping system. Pioneer studies demonstrated a participation of the heat shock factor 1 (HSF1)[2] and cold-inducible RNA binding protein (CIRP)[8] in the mechanism of temperature clock entrainment. However, functional inhibition of HSF1 or CIRP does not completely inhibit temperature entrainment,[2,8,9] suggestive of a yet-unidentified additional mediator(s) playing a role in temperature entrainment.[10] Physiological body temperature only changes modestly and gradually over the course of 24 h, raising the question of how this modest signal effectively adjusts molecular clock oscillations.

Given that a considerable proportion of protein synthesis in cells undergoes circadian variation,[11,12] temperature may affect mRNA translation. Among the diverse elements in mRNAs such as primary and secondary structures in the 5′ and 3′ untranslated regions (UTRs), a small open reading frame (ORF) present upstream of the main ORF is a widespread regulatory motif in transcriptomes.[13,14] Upstream ORFs (uORFs) typically repress translation from the downstream main ORF, trapping the 5′ to 3′ scanning of the pre-initiation ribosome complex before it reaches the start codon in the main ORF.[13,14] Although most uORFs

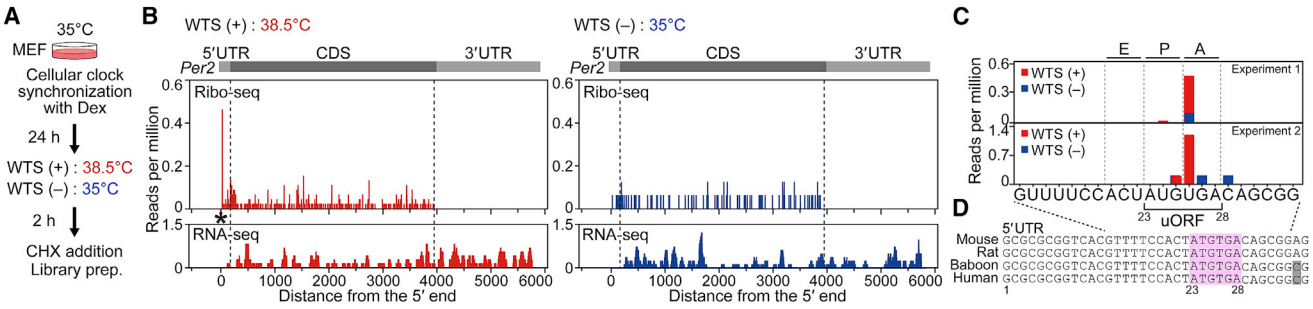

Figure 1. Identification of a temperature-responsive uORF in the circadian core clock gene *Per2*

(A) Schematic experimental design for ribosome profiling. Dex, dexamethasone.

(B) Distribution of ribosome footprints along the *Per2* gene (representative of three biological replicates). Asterisk, uORF in the *Per2* 5′ UTR.

(C) Ribo-seq profiles of biological replicate samples, showing WTS-induced accumulation of footprints in the *Per2* uORF.

(D) Conserved uORFs in *Per2* 5′ UTRs of human, mouse, rat, and baboon. Numbers on the alignment indicate positions relative to the mouse *Per2* transcription start site.

encode a significant length of the polypeptide, minimal uORFs (m-uORFs), which just bear AUG start codon and stop codon, have been reported to function in a different manner than typical uORFs.[15] In plants, m-uORFs were identified as borate-induced ribosome stalling sites; these are needed for physiological response to environmental boron availability.[15] Apart from plants, however, although m-uORFs were identified in mammalian genome sequences including those in humans and mice,[16,17] their specific roles in physiology are still ill-defined.

Here, we have identified a functional m-uORF in the 5′ UTR of the core clock gene *Per2*. *Per2* is a robustly oscillating clock gene and is essential for driving molecular clock oscillations.[18–21] We examined the role played by the *Per2* m-uORF in the temperature-dependent clock entrainment mechanism. Our data describe a previously uncharacterized functional link between uORF and circadian clock.

RESULTS

The *Per2* uORF binds ribosomes at increased temperature

To analyze the potential effect of a physiological warm temperature shift (WTS) (35°C–38.5°C) on *Per2* transcription and translation in mammalian cells, we performed RNA-seq and Ribo-seq on dexamethasone-synchronized mouse embryonic fibroblasts (MEFs) with or without WTS at the circadian rising phase of Per2. We treated confluent cells with dexamethasone to synchronize their endogenous circadian clocks for 24 h, and subsequently performed a WTS for 2 h, when endogenous Per2 protein expression is upregulated by circadian mechanisms[21] (Figure 1A). Under these conditions, we found a quantifiable accumulation of ribosomes at the 5′ flanking region of the main coding sequence of *Per2* mRNA in WTS-treated cells (Figure 1B, WTS(+), asterisk). On the other hand, in control cells cultured at a constant temperature (WTS(–)), these 5′ UTR signals were scarcely detected (Figure 1B, WTS(–)). RNA-seq signals were comparable between WTS-treated and untreated cells (Figure 1B, lower tracks). Similar temperature-dependent ribosomal accumulation at the 5′ UTR was observed consistently in three different sets of experiments (GSE188529). Sequencing data from all sets showed that 5′ UTR ribosomal accumulation occurred on an AUG-UGA minimum ORF, in which the start codon is directly followed by a stop codon, with consensus P- and A-sites located in-frame at AUG and UGA, respectively (Figure 1C). This m-uORF sequence located upstream of the *Per2* CDS, hereafter referred to as *Per2* m-uORF, is highly conserved among mammalian species including humans and mice (Figures 1D and S1A).

Temperature-dependent Per2 change depends on the *Per2* m-uORF but not *Per2* transcription

A physiological temperature might modulate the oscillating levels of the endogenous Per2 protein. To test this, we performed protein blot analysis using cells treated with WTS at 0, 4, 8, 12, 16, 20, 24, and 28 h after synchronization (Figure 2A), and we found the capability of WTS to increase Per2 protein expression in a manner depending on the time of WTS applied. When applied at time 0, 4, 20, 24, and 28, which correspond to the Per2 protein rising phase, WTS led to a greater Per2 expression (Figure 2A, see arrowheads: at each time point, a greater increase was observed in the lower band, which most likely corresponds to non-phosphorylated nascent Per2 proteins as we and others reported[19,22]). WTS had no effect on the expression of Per2 during its declining phase, at time 8, 12, or 16. WTS did not influence the expression of α-tubulin, nor of other clock proteins (Figure S2A). Immunoblots of Per2 protein from mouse lung and skin cultures in the presence or absence of WTS (Figure S2B) reproduced the temperature-dependent increase in endogenous Per2 protein abundance. [^{35}S]methionine or click-labeling experiments analyzing de novo protein synthesis (Figures 2B and S2C) and the results from polysome profiling, which indicated *Per2* mRNA association to heavier polysomes upon WTS (Figure 2C), corroborated the increase in Per2 protein synthesis in cells after WTS.

Despite the change of Per2 expression by WTS, *Per2* transcripts were nearly unaffected by the same treatment at any time points tested (Figure 2A, right lower panel), making it unlikely that transcriptional regulation underlies this response. This was further supported by limited or no effect of WTS on transcription through the heat shock element, cAMP/Ca^{2+} response

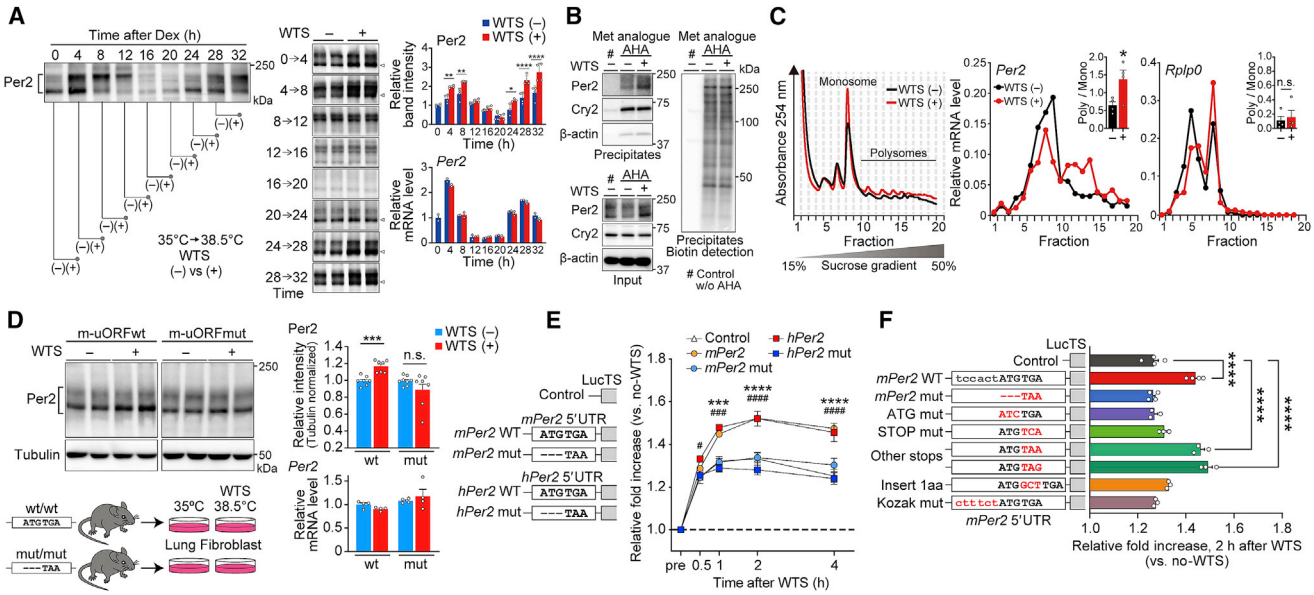

Figure 2. *Per2* minimal uORF mediates temperature-dependent Per2 protein translation

(A) Left, Per2 protein accumulation in the presence or absence of WTS at multiple circadian time points in Dex-synchronized MEFs. n = 4 biological replicates. Right, protein and mRNA quantification data (from two independent experiments). Error bars indicate SD.

(B) Immunoblots of newly synthesized Per2 protein labeled by click chemistry. Biotin-labeled proteins were purified and probed for either Per2 or biotin.

(C) Representative polysome profiles (left) and qRT-PCR data (center [*Per2*] and right [*Rplp0*]) of WTS-treated or untreated MEFs. Insets show polysome-to-monosome ratios. n = 4 biological replicates.

(D) Immunoblots showing WTS-dependent accumulation of Per2 protein in WT and *Per2* m-uORF mutant mouse lung fibroblast (MLFs). Bar graphs show relative abundance of Per2 protein and mRNA (n = 7–8 and 4 biological replicates, respectively).

(E) Luciferase reporter activity traces of *Per2* m-uORF-dependent translation after WTS. n = 4 biological replicates. ***p < 0.001, ****p < 0.0001 (control vs. mPer2 WT); #p < 0.05, ###p < 0.001, ####p < 0.0001 (control vs. hPer2 WT). Luc-TS, thermostable luciferase.

(F) Fold increase of WT and different mutant series of the *Per2* m-uORF. n = 3–4 biological replicates. Data in (C) and (D) were analyzed using the unpaired two-sided Student's t test; in (A) and (E), two-way ANOVA followed by Holm-Sidak *post hoc* tests; in (F), one-way ANOVA followed by Tukey's multiple comparisons test. Values are means ± SEM; *p < 0.05, **p < 0.01, ***p < 0.001, ****p < 0.0001, otherwise indicated.

element, and serum response element, which are known to affect *Per2* gene transcription through its promoter[23–25] (Figures S2D and S2E). WTS had no significant effect on the intracellular localization of *Per2* transcripts (Figure S2F). Per2 protein stability (or protein degradation rate), assessed by cycloheximide treatment, was nearly unchanged upon WTS (Figure S2G). These results strongly suggest that a mild temperature change (which differs from heat shock stress) affects Per2 abundance mainly via regulated translation.

Primary mouse lung fibroblasts were next prepared from wild-type (WT) mice and newly generated *Per2* m-uORF mutant (mut) mice (Figure S3A), in which the original *Per2* ATG-TGA sequence had been mutated to TAA. Notably, in *Per2* m-uORF mut cells, WTS did not alter Per2 expression (p = 0.3864, WTS(+) vs. WTS(–) in mut cells; p = 0.0005 for WT cells, Figure 2D). In both basal and WTS-treated cells, *Per2* transcript levels were comparable between the WT and m-uORF mut cells (Figure 2D), excluding a possible effect on *Per2* transcription by the mutation. In addition, the normal circadian locomotor activity rhythm and unimpaired clock gene expressions in liver and lung exhibited by the mut mice kept under constant darkness (DD) (Figures S3B–S3E) suggest that removal of the *Per2* m-uORF is not deleterious for circadian rhythm generation under steady-state conditions. Rather, this 5′ UTR sequence appears to have a more limited role in modulating Per2 expression in response to temperature.

The function of the *Per2* m-uORF sequence was next examined further using reconstituted luciferase reporters. The region of the human and mouse *Per2* 5′ UTR containing the m-uORF sequence, cloned into a reporter vector with a thermostable version of firefly luciferase[26] (Figure S4A), conferred a WTS response to the reporter (see Figure 2E, ~70% increase compared with no *Per2* 5′ UTR vector). The response was absent in constructs in which the m-uORF was mutated from ATGTGA to TAA (see also Figure S4B). Disruption of the m-uORF structure by means of ATG mutation, stop codon mutation, or extra codon insertion between ATG and TGA also abolished responsiveness to WTS, as did disruption of the Kozak sequence upstream of the m-uORF (Figures 2F and S4B). These data indicate that the isolated *Per2* 5′ UTR containing the m-uORF suffices to impart temperature dependence to the downstream reporter translation.

Blocking phosphoinositide 3-kinase abrogates the WTS response of Per2 expression

Potential molecular mediator(s) involved in the WTS response of Per2 expression was next explored pharmacologically. We generated Per2::LucTS knockin MEF cells, in which the

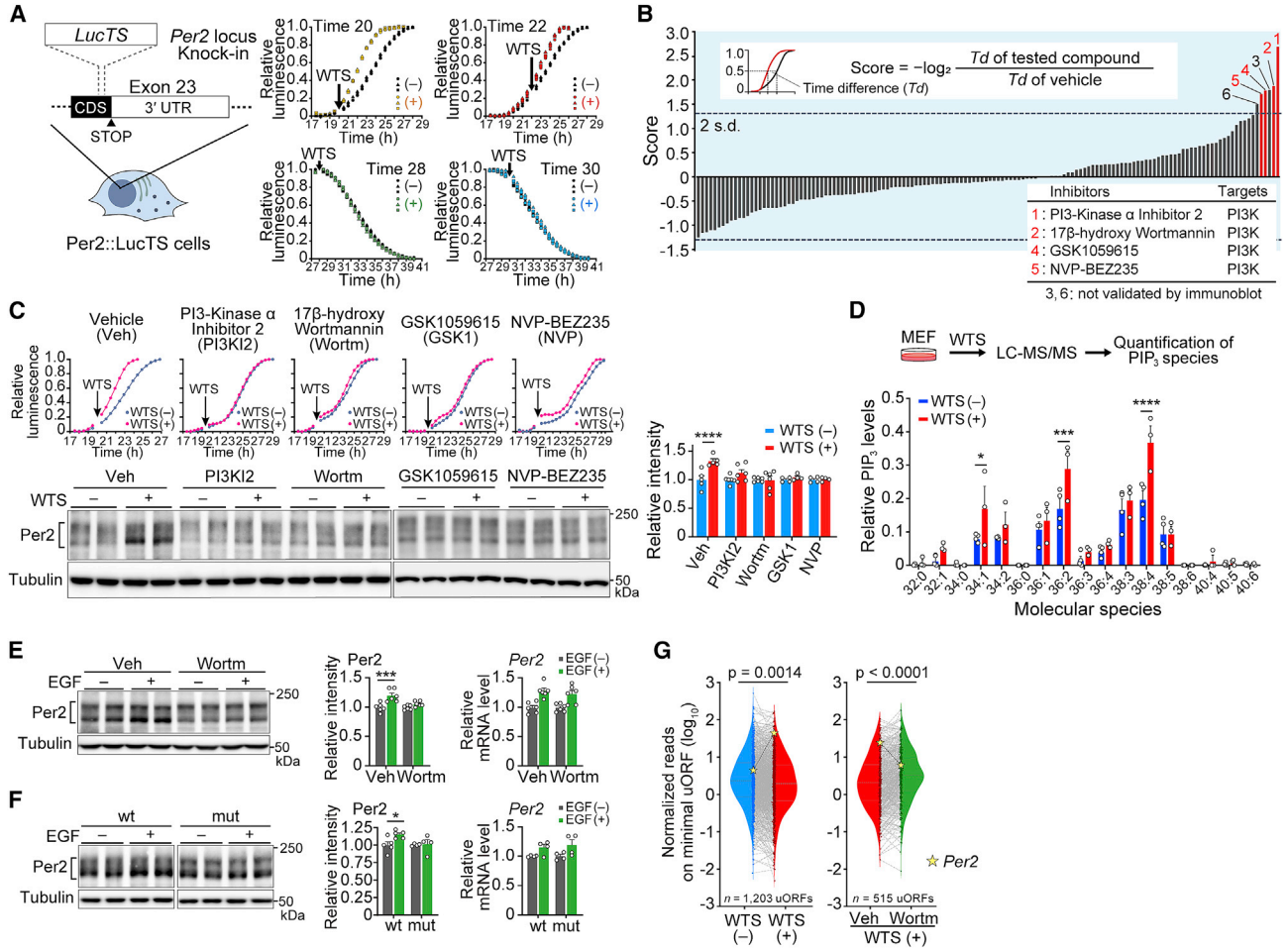

Figure 3. PI3K mediates the temperature response of Per2 translation

(A) Reporter activity traces of Per2::LucTS knockin cells with or without WTS during rising (time 20, 22) and declining (time 28, 30) phases of Per2 expression. Data are from three biological replicates.

(B) Kinase inhibitor screening identifying a key mediator of WTS-dependent Per2 translation. Horizontal dashed line, threshold of 2 SD. Red, PI3K inhibitors.

(C) Per2::LucTS traces showing the effects of PI3K inhibitors on WTS-dependent Per2 translation. Cells were subjected to WTS at time 20 with or without the indicated PI3K inhibitors. Western blots show the expression of the endogenous Per2. n = 4–6 biological replicates.

(D) Mass spectrometry profiling of PIP_3 species in cultured MEFs with or without WTS. n = 3–4 biological replicates.

(E) EGF-induced increase of Per2 protein accumulation and its inhibition by Wortm. Per2 protein and mRNA quantification are shown on the right. Cells were treated with EGF for 2 h. n = 6 biological replicates.

(F) Immunoblots showing EGF-dependent Per2 protein accumulation in WT and *Per2* m-uORF mutant MLFs. n = 4–5 biological replicates.

(G) Metagene Ribo-seq violin plots showing the effects of WTS and Wortm on ribosome accumulation on minimum uORFs. Each dot indicates the read count for an individual minimal uORF normalized to its gene expression level. Data were averaged from two (right) or three (left) biological replicates. Star indicates *Per2*. All data plotted are available in Table S1. Data in (C)–(F) were analyzed using two-way ANOVA followed by Sidak's multiple comparisons test; in (G), the Mann-Whitney U test. Values are means ± SEM; *p < 0.05, ***p < 0.001, ****p < 0.0001.

thermostable luciferase[26] (LucTS) was fused to endogenous Per2 (Figure 3A). This knockin LucTS activity recapitulated Per2 expression in terms of both its circadian-rising phase-specific increase in reaction (Figure 3A) and sensitivity to WTS (Figure S4C).

Examination of ~150 kinase inhibitors (Cayman library) and follow-up validation by western blot analysis identified four compounds that abrogated the response of the endogenous Per2 protein expression to WTS (Figures 3B, 3C, and S4D). Notably, all four inhibitors shared a single target, i.e., phosphoinositide 3-kinase (PI3K), which has been implicated in cellular heat stress signaling.[27–29] This result prompted us to assay for PI3K in the context of WTS signaling. The primary product of PI3K, phosphatidylinositol 3,4,5-trisphosphate (PIP_3), identified by LC-MS, was increased in response to WTS (Figures 3D, S4E, and S4F). The specific PI3K inhibitor 17β-hydroxy wortmannin (Wortm) blocked this upregulation of PIP_3. Moreover, Wortm blocked the response of Per2 to WTS in a dose-dependent manner with an IC_{50} of ~20 nM, similar to previous studies[30,31] (Figure S4G).

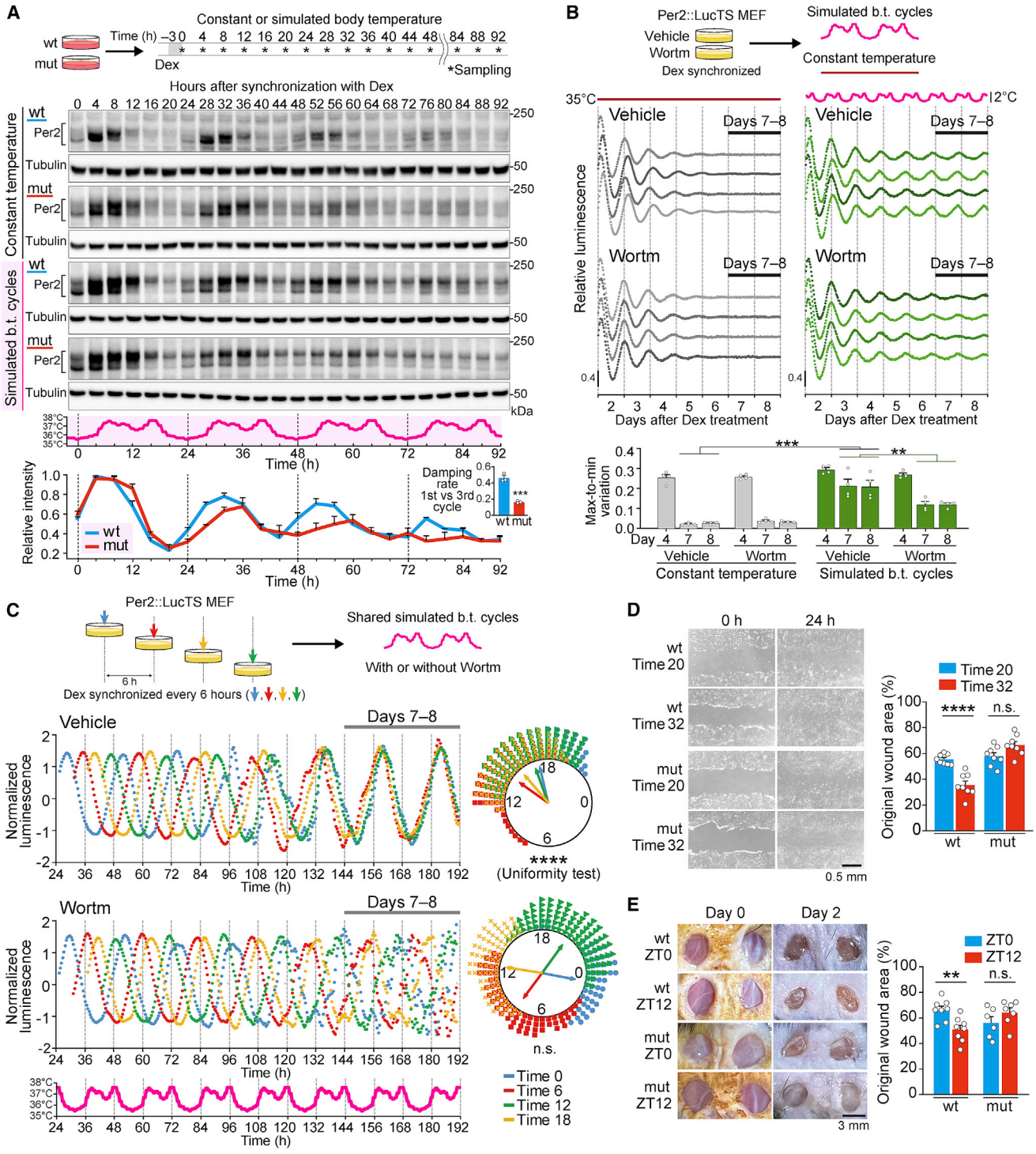

Figure 4. *Per2* uORF is essential for circadian temperature entrainment

(A) Representative temporal profiles and quantification of Per2 protein expression in WT and *Per2* m-uORF mut MLFs with or without simulated body temperature cycles. Cells were sampled every 4 h over 4 consecutive days. n = 3 biological replicates. All immunoblot images are provided in Figure S6. Inset bar graph shows damping in the third cycle relative to the first cycle.

(B) Temperature cycle-dependent circadian sustainability in Per2::LucTS cells in the presence or absence of Wortm. Raw data were detrended by 24-h moving average and expressed relative to the first peak value of luminescence. Bottom, graphs of daily max-to-min variance for days 4, 7, and 8. n = 4 biological replicates.

(legend continued on next page)

To test further our PI3K-Per2 axis model, we sought to activate PI3K using an alternative stimulus. For this, we used the epidermal growth factor (EGF), which is known to function as a potent PI3K activator[32] and has been shown to enhance Per2 expression at the transcriptional and the protein translation level via a yet unknown mTOR-independent pathway.[33] We observed that the *Per2* m-uORF was required for EGF treatment-induced Per2 expression, which also relies on PI3K activation (Figures 3E and 3F). The shared requirement of the *Per2* m-uORF for the WTS and EGF treatment-induced promotion of Per2 protein expression, both requiring PI3K, supports the hypothesis that PI3K is lying in a crossroads linked to the *Per2* m-uORF-mediated Per2 expression. We confirmed that *Per2* mRNA levels were equivalent between WT and mut cells before and after EGF treatment (Figures 3E and 3F).

To consolidate the suggested link between PI3K and *Per2* m-uORF, ribosome profiling was performed using cells subjected to WTS in the presence or absence of Wortm (Figure 3G). The WTS-induced 5′ UTR ribosome accumulation signal on the *Per2* m-uORF (Figures 3G, left and 1C) was reduced in cells to which Wortm was co-applied (Figures 3G, right and S1B), depicting the necessity of PI3K to cause WTS-induced ribosome binding to the *Per2* m-uORF. All data plotted in Figure 3G are available in Table S1.

We examined inhibitors toward mTOR (rapamycin),[33] Akt (MK2206), MEK (U0126), HSF-1 (KNK437),[2,9] TRP channel (Ru red), m6A methylation pathway (DZnep),[34,35] and CK1 (D4476),[36,37] but none of these displayed an inhibitory effect on the WTS response of Per2::LucTS activity (Figure S4H). PI3K inhibition thus appears to be unique in strongly diminishing the Per2 WTS response.

The *Per2* m-uORF and PI3K mediate circadian clock temperature entrainment

Because the body temperature cycle over time is a continuous function and not a square wave, we tested the cellular response to thermal cycles that more closely resembled body temperature fluctuations (Figures 4 and S6). Using telemetry, we measured murine abdominal body temperatures and calculated a mean 24 h profile.[38] Cells were synchronized using dexamethasone, then released into either constant (35°C) or simulated body temperature conditions over 92 h. As reported previously,[1] this temperature profile enhanced the rhythm amplitude of Per2 protein expression over four circadian cycles in WT cells (Figures 4A and S6). In contrast, the body temperature profile did not efficiently enhance the rhythm sustainability of Per2 protein expression in *Per2* m-uORF mut cells (Figure 4A), with the first vs. third cycle damping rate being significantly lower than that of WT cells (Figure 4A, inset). The initiation of Per2 protein expression after dexamethasone treatment was similar between WT and mut cells. The damping rates of the two genotypes were also similar in constant temperature conditions (Figures 4A and S6). Thus, Per2 expression rhythms in mut cells were basically normal, whereas these cells did not show an efficient enhancement of Per2 protein expression rhythm in response to temperature.

Consistent with our hypothesis of the PI3K-*Per2* m-uORF axis, Wortm significantly attenuated the amplitudes of Per2::LucTS rhythms under simulated body temperature cycles by days 7 and 8 (vehicle vs. Wortm, $p = 0.0045$ on day 7, $p = 0.0078$ on day 8, Figure 4B). However, although attenuated, a clear residual rhythm remained after Wortm treatment, suggesting the participation of additional regulatory factor(s) in maintaining Per2 expression-cycle amplitude. Because the CIRP is a possible additional mediator of circadian regulation[8,39] and we observed that a mild down-shift in temperature (from 38.5°C to 35°C) caused induction of *Cirp* mRNA expression but not of *Per2*/Per2 expression in cells we used (Figure S5A), and that the simulated body temperature cycles drove fluctuating *Cirp* mRNA expression in our Wortm-treated cells (Figure S5B), we performed knockdown of *Cirp*. The knocking down of *Cirp* in conjunction with Wortm treatment led to a more severe defect in Per2::LucTS rhythmicity (Figures S5C and S5D). Thus, it appears that both PI3K and *Cirp* are involved in maintaining rhythmic Per2 protein expression under simulated circadian body temperature cycles.

A stronger Wortm effect was observed when re-entrainment to a new temperature cycle was examined (Figure 4C). We prepared Per2::LucTS cell cultures in different phases that were separately synchronized using dexamethasone at 6 h intervals and subjected to simulated body temperature cycles with a shared synchronous phase. After several days in culture, Per2::LucTS rhythmic expression adapted to the shared simulated body temperature cycles. In Figure 4C, to emphasize the phase of the rhythms, the values were normalized using 24 h SD of luminescence. By days 7–8, the phases of all tested cultures converged (Figure 4C, upper), resulting in a significant increase in phase uniformity (Rayleigh's uniformity test, $p < 0.0001$). In contrast, when the cells were cultured with Wortm, the temperature cycles no longer robustly synchronized phases of Per2::LucTS rhythms (Figure 4C, lower), and the day 7–8 phases remained diverged (Rayleigh's uniformity test, $p = 0.999$). These results demonstrate that PI3K-mediated signaling is indispensable for phase entrainment by simulated physiological body temperature cycles.

(C) Thermal entrainment of Per2::LucTS bioluminescence in the presence and absence of Wortm. Cells were synchronized by Dex every 6 h around the circadian cycle and released into a common simulated body temperature cycle. To emphasize the phase of rhythms, amplitudes were normalized using 24-h moving SD of the detrended luminescence. Rayleigh plots show phase distribution of acrophase, defined as >0.7 of normalized amplitude, on days 7–8. Plots are color coded according to Dex synchronization time, each representing two biological replicates. Arrows in the circles are Rayleigh plot vectors.

(D) Circadian wound-healing responses of fibroblast monolayers derived from WT or *Per2* m-uORF mut mice. Graphs show wound areas at 24 h relative to initial wound areas at 0 h. n = 8 biological replicates.

(E) *In vivo* wound healing in WT and *Per2* m-uORF mut mice. Bar graphs show wound areas relative to initial wound areas on day 0. n = 6–8 mice. Data in (A) were analyzed by unpaired two-sided Student's t test; in (B), three-way ANOVA followed by Tukey *post hoc* tests; in (C), Rayleigh's uniformity test; in (D) and (E), two-way ANOVA followed by Sidak's multiple comparisons test. Values are means ± SEM; $^{**}p < 0.01$, $^{***}p < 0.001$, $^{****}p < 0.0001$; n.s., not significant.

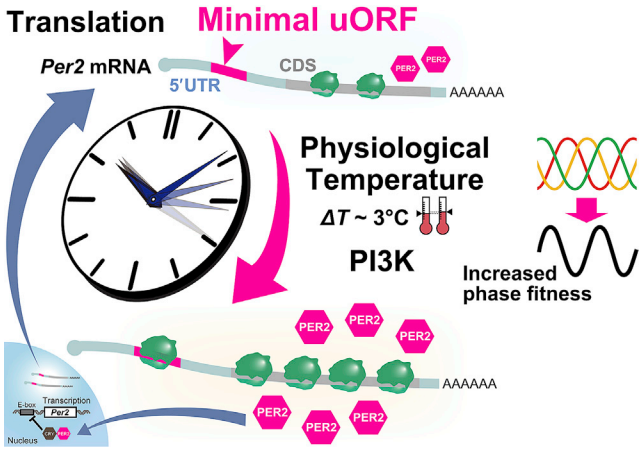

Figure 5. A model depicting a role of *Per2* m-uORF in circadian clock entrainment

Per2 minimal uORF located in the 5′ UTR of *Per2* mRNA contributes to the circadian clock phase adaptation toward day/night physiological body temperature rhythms via the PI3K-uORF pathway; this adaptation is indispensable for maintaining optimal tissue homeostasis.

The physiological contribution of the *Per2* m-uORF to circadian skin regeneration

Temperature-dependent phase fitness of the clock may have a role in shaping circadian physiology. To gain experimental insight into this possibility, we assessed the day/night wound healing activity rhythm reported for skin, a tissue controlled by body temperature rhythms.[40] We performed wound-scratch tests using synchronized monolayers of primary skin fibroblasts under simulated body temperature conditions (Figure 4D). Skin fibroblasts prepared from WT mice exhibited circadian variations in the residual wound area after 24 h of healing. In good agreement with previous reports,[41] wounds inflicted at the peak of Per2 expression (time 32) healed more efficiently than those inflicted at the trough of Per2 expression (time 20). However, cells prepared from *Per2* m-uORF mut mice show delayed wound healing at time 32, resulting in blunted time dependency (Figure 4D). We also wounded the skin of adult mice at the beginning of their resting or active phase (ZT0 or 12) and allowed them to heal for 2 days (Figure 4E). In WT mice, greater healing was observed for wounds made at ZT12 than at ZT0, a result compatible with that reported previously.[41] However, no significant difference was observed between ZT0 and ZT12 in mut mice, indicating that the m-uORF is required to shape the time-dependent healing response.

DISCUSSION

m-uORFs represent the shortest uORFs that can be found in the 5′ UTRs of certain eukaryotic mRNAs. Although minimal-type uORFs in mouse and human transcriptomes have been identified earlier,[16,17] their specialized role(s) in physiology has remained elusive. In this study, we identified a functional m-uORF in the 5′ UTR of the core clock gene *Per2* and uncovered its role as a post-transcriptional phase-tuning module for circadian clock entrainment. The AUG-stop *Per2* m-uORF sequence, which we identified as a temperature-sensitive element by ribosome profiling, contributed to circadian time-dependent and transcription-independent upregulation of Per2 protein synthesis by temperature. Pharmacological screening helped identify PI3K as the principal molecular mediator for temperature-dependent *Per2* m-uORF regulation and Per2 protein expression, although the precise mechanism by which PI3K regulates Per2 is unknown in our study. We observed that cells oscillating with different phases became synchronized after several days in simulated body temperature cycles, verifying temperature as a potent phase-synchronizer of cellular clocks. Inactivation of the PI3K-*Per2* m-uORF axis severely compromised this physiological temperature cycle-driven synchronization. Using skin as a model system, we showed that *Per2* m-uORF-mediated regulation is required for optimal wound healing. Our data therefore revealed a previously uncharacterized functional link between uORF and circadian clock. The m-uORF in *Per2* mediates circadian clock phase adaptation to day/night physiological body temperature rhythm and contributes to enhancing circadian clock-associated tissue homeostasis (Figure 5, model).

There are conceivable teleological benefits in having a translation-based control, alongside transcriptional regulation, with regard to *Per2*/Per2 regulation: temporally, body temperature rises near the beginning of behaviorally active phase, which coincides with increasing Per2 protein translation (but not transcription) from its mRNA. Translation relies on mRNA abundance, which for *Per2* cycles robustly; thus, the Per2 WTS response is highly phase dependent, which has utility for participating in phase-dependent phase entrainment, a hallmark of the circadian clock system.[2] Having a separate layer of regulation, at the translation level, itself, might be advantageous in increasing the fitness (or, phase plasticity) of circadian clock mechanisms that rely on both cyclic transcription and translation.[12,42,43]

Using reporter assays, we found that the minimum AUG-stop structure of the *Per2* m-uORF is critical in inducing the WTS response, although the precise underlying mechanisms are unclear. Owing to its minimal nature, no peptide is produced from the m-uORF. Ribosomes were found on the *Per2* m-uORF, with their P- and A-sites at the start and stop codons, respectively, implying combinatory recruitment of initiation- and termination-related factors. No ribosomal translocation occurs in this site, indicating the absence of nascent peptides inside the ribosomal exit tunnel, a structure also unique to the m-uORF. How these above-mentioned features relate to the *Per2* WTS response is our next question. In this respect, it may be worth mentioning that stalled ribosomes are reported to recruit additional factors to regulate CDS translation.[44] Because similar WTS-dependent ribosome accumulation and PI3K dependency were detected for other 62 m-uORFs (see details in Table S1), including *Drosha*, *Dopey2*, and *Plekha2* (Figure S1C), and that WTS-induced expression was also recapitulated by a LucTS reporter containing m-uORFs from *Drosha* and *Dopey2* but not *Plekha2* (Figure S1D), it is interesting to see whether these or some of the m-uORFs share a similar role. A study reported that *Drosha* expression can be translationally regulated via a mechanism involving the m-uORF.[44]

The *Per2* m-uORF and its surrounding sequence are highly conserved among mammals, but not in birds, reptiles,

amphibians, fish, or insects. The platypus, an animal belonging to the mammals but deficient in heat-producing brown adipose tissue (BAT), lacks the *Per2* m-uORF (see Figure S1A), suggesting the idea of *Per2* m-uORF being a late in evolution fine-tuning mechanism for BAT-containing homeotherms; the range of evolutionary conservation of the *Per2* m-uORF mechanism, however, remains to be determined.

PI3K has been shown to be activated by heat shock stress.[27,28] In this study, we observed that a mild temperature change can also activate PI3K, and this finding is compatible with that from other studies.[29,45] It is presently unknown whether heat shock and WTS use the same mechanism. Thermal sensor(s) responsible for the observed activation may exist upstream of PI3K. PI3K itself may function as a thermosensitive enzyme. Temperature may also affect cell membrane fluidity,[46] influencing the interaction between PI3K and its substrate PIP_2. Addressing this question is our next challenge. We should also solve the question of whether and how the m-uORF-dependent translational mechanism acts in concert with other known thermal clock entrainment mechanisms, including those involving HSF1[2,9] and CIRP.[8] Translational regulation of other clock genes also requires further investigation.[11,12] Addressing how these different types of (post-)transcriptional and translational mechanisms coordinate to regulate circadian timekeeping system will be important to understand organism-wide phase fitness of circadian clock-regulated physiology.

In mammals, the organismal circadian timing system is organized in a hierarchy of multiple oscillators. The master clock resides in the suprachiasmatic nucleus (SCN) in the brain, while numerous peripheral tissues possess their own clocks, constituting a hierarchical, but adaptive multi-oscillator system.[5] One requirement of this network model is the existence of endogenous signals through which the peripheral clocks adjust their pace and phase according to the rhythm imposed by the SCN. Importantly, body temperature plays this part.[2,4,5] In this study, we found that temperature entrainment mechanism employs a post-transcriptional regulatory mechanism involving the minimal-type uORF of the core clock gene *Per2*. To our surprise, this translation-based mechanism allows cellular clocks to adapt to innocuous temperature cycles. As changes in physiological body temperature are modest and gradual, this adaptive regulation of Per2 protein expression may be important to manipulate phase fitness of circadian clock-related physiology.

Limitations of the study

As observed in *Per2* m-uORF mut mice, an impaired wound healing also occurs as a result of *Cry1/2* deficiency[41] and *Per1/2* mutation[47]; however, it is not known (and there is no literature answering) whether clock gene expression—Per2 in our study—is directly impacted by wound healing in a time-dependent manner. Our attempt to detect the potential Per2 expression change by immunohistochemistry was unsuccessful due in part to the tissue complexity of the wounded area.[48] In addition, cell division itself is a perturbing factor for Per2/clock oscillation.[49,50] Nevertheless, given that not only EGF but also FGF, PDGF, and VEGF, all known to activate PI3K, operate during wound healing,[51] a more rigorous analysis such as that using a recently developed single-cell-based Ribo-seq[52] and/or FACS-based cell-type-specific mass spectrometry analysis will be required to overcome our limitation.

Our simulated body temperature experiments provide a starting point in understanding the role(s) of *Per2* m-uORF in circadian biology. Our data showed that this element is apparently dispensable for keeping normal circadian clock gene expression in peripheral tissues *in vivo*. Relatedly, genetic ablation of glucocorticoid-glucocorticoid receptor pathway, which has been regarded crucial for peripheral clock entrainment, had no marked effect on the rhythms in periphery under normal LD or DD conditions, because many parallel routes are employed to synchronize these peripheral clocks *in vivo*.[4,53,54] Under high-fat diet conditions, the body weight of WT and *Per2* m-uORF mut mice increased similarly (Figures S3F and S3G); thus, the *Per2* m-uORF is dispensable for body weight homeostasis at least under chronic high-fat diet conditions. Nevertheless, other metabolic perturbations such as daytime feeding and/or exercise, known to influence body temperature, would merit further investigation.[55–57] We showed that both *Per2* m-uORF and *Cirp* are involved in maintaining high-amplitude rhythmic Per2 protein expression under simulated body temperature cycles *in vitro*. In cultured cells, HSF1 also contributes to the temperature entrainment of the molecular clock.[8,9] However, currently, the roles of CIRP and HSF1 in the peripheral tissue clock synchronization *in vivo* remain unclarified. Thus, a significant limitation of our study is that, even though we used simulated body temperature cycles, we cannot approach the extent of impact of *Per2* m-uORF *in vivo* by our study. Combined inactivation of *Cirp*/*Hsf1* and *Per2* m-uORF may be required to investigate the temperature entrainment system in the organism.

STAR★METHODS

Detailed methods are provided in the online version of this paper and include the following:

- KEY RESOURCES TABLE
- RESOURCE AVAILABILITY
  - Lead contact
  - Materials availability
  - Data and code availability
- EXPERIMENTAL MODEL AND SUBJECT DETAILS
  - Cell lines
  - Mice
  - Primary fibroblasts
- METHOD DETAILS
  - Temperature control
  - Ribo-seq and RNA-seq analysis
  - Polysome profiling
  - Immunoblotting
  - Labeling of de novo protein synthesis
  - LucTS reporter assay
  - Per2::LucTS cell-based kinase inhibitor assay
  - Quantification of PIP_3 species
  - Quantitative RT-PCR
  - AAV-mediated gene knockdown
  - *In vitro* and *in vivo* wound assay

- Locomotor activity recording
- High fat diet feeding

- QUANTIFICATION AND STATISTICAL ANALYSIS

SUPPLEMENTAL INFORMATION

Supplemental information can be found online at https://doi.org/10.1016/j.celrep.2023.112157.

ACKNOWLEDGMENTS

We thank Ms. Mari Mito (RIKEN Cluster for Pioneering Research) for technical assistance. This work was supported in part by research grants from the Ministry of Education, Culture, Sports, Science and Technology of Japan (22H04987, 20H05783, and 20K21426 to M.D.; 16H06276 and 22K15274 to T.M.; 20H05784 to S.I.; 21H05734 to Y.S.), the Basis for Supporting Innovative Drug Discovery and Life Science Research program of the Japan Agency for Medical Research and Development (JP21am0101092), the Kusunoki 125 of Kyoto University 125th Anniversary Fund, and the Kobayashi Foundation (to M.D.), as well as the Narishige Neuroscience Research Foundation, the Tokyo Biochemical Research Foundation, the Takeda Science Foundation, and the Kato Memorial Bioscience Foundation (to T.M.).

AUTHOR CONTRIBUTIONS

Conceptualization, M.D.; methodology, Y.S., J.S., T. Sasaki, S.I., and M.D.; investigation, T.M., Y.I., X.S., T. Seta, Y.A., K.T.N.P., Y.S., J.S., T. Sasaki, Y.Y., H.O., S.I., and M.D.; writing – original draft, T.M., Y.I., S.I., and M.D.; writing – review & editing, T.M., Y.I., and M.D.; funding acquisition, T.M., Y.S., S.I., and M.D.; resources, M.I. and M.D.; supervision, M.D.

DECLARATION OF INTERESTS

The authors declare no competing interests.

Received: September 14, 2022
Revised: December 29, 2022
Accepted: February 9, 2023
Published: March 6, 2023

REFERENCES

1. Brown, S.A., Zumbrunn, G., Fleury-Olela, F., Preitner, N., and Schibler, U. (2002). Rhythms of mammalian body temperature can sustain peripheral circadian clocks. Curr. Biol. *12*, 1574–1583. https://doi.org/10.1016/s0960-9822(02)01145-4.
2. Buhr, E.D., Yoo, S.H., and Takahashi, J.S. (2010). Temperature as a universal resetting cue for mammalian circadian oscillators. Science *330*, 379–385. https://doi.org/10.1126/science.1195262.
3. Patke, A., Murphy, P.J., Onat, O.E., Krieger, A.C., Özçelik, T., Campbell, S.S., and Young, M.W. (2017). Mutation of the human circadian clock gene CRY1 in familial delayed sleep phase disorder. Cell *169*, 203–215.e13. https://doi.org/10.1016/j.cell.2017.03.027.
4. Asher, G., and Schibler, U. (2011). Crosstalk between components of circadian and metabolic cycles in mammals. Cell Metab. *13*, 125–137. https://doi.org/10.1016/j.cmet.2011.01.006.
5. Schibler, U., Gotic, I., Saini, C., Gos, P., Curie, T., Emmenegger, Y., Sinturel, F., Gosselin, P., Gerber, A., Fleury-Olela, F., et al. (2015). Clock-talk: interactions between central and peripheral circadian oscillators in mammals. Cold Spring Harb. Symp. Quant. Biol. *80*, 223–232. https://doi.org/10.1101/sqb.2015.80.027490.
6. Welz, P.S., Zinna, V.M., Symeonidi, A., Koronowski, K.B., Kinouchi, K., Smith, J.G., Guillén, I.M., Castellanos, A., Furrow, S., Aragón, F., et al. (2019). BMAL1-driven tissue clocks respond independently to light to maintain homeostasis. Cell *177*, 1436–1447.e12. https://doi.org/10.1016/j.cell.2019.05.009.
7. Man, K., Loudon, A., and Chawla, A. (2016). Immunity around the clock. Science *354*, 999–1003. https://doi.org/10.1126/science.aah4966.
8. Morf, J., Rey, G., Schneider, K., Stratmann, M., Fujita, J., Naef, F., and Schibler, U. (2012). Cold-inducible RNA-binding protein modulates circadian gene expression posttranscriptionally. Science *338*, 379–383. https://doi.org/10.1126/science.1217726.
9. Saini, C., Morf, J., Stratmann, M., Gos, P., and Schibler, U. (2012). Simulated body temperature rhythms reveal the phase-shifting behavior and plasticity of mammalian circadian oscillators. Genes Dev. *26*, 567–580. https://doi.org/10.1101/gad.183251.111.
10. Kornmann, B., Schaad, O., Bujard, H., Takahashi, J.S., and Schibler, U. (2007). System-driven and oscillator-dependent circadian transcription in mice with a conditionally active liver clock. PLoS Biol. *5*, e34. https://doi.org/10.1371/journal.pbio.0050034.
11. Janich, P., Arpat, A.B., Castelo-Szekely, V., Lopes, M., and Gatfield, D. (2015). Ribosome profiling reveals the rhythmic liver translatome and circadian clock regulation by upstream open reading frames. Genome Res. *25*, 1848–1859. https://doi.org/10.1101/gr.195404.115.
12. Castelo-Szekely, V., Arpat, A.B., Janich, P., and Gatfield, D. (2017). Translational contributions to tissue specificity in rhythmic and constitutive gene expression. Genome Biol. *18*, 116. https://doi.org/10.1186/s13059-017-1222-2.
13. Hinnebusch, A.G., Ivanov, I.P., and Sonenberg, N. (2016). Translational control by 5′-untranslated regions of eukaryotic mRNAs. Science *352*, 1413–1416. https://doi.org/10.1126/science.aad9868.
14. Zhang, H., Wang, Y., and Lu, J. (2019). Function and evolution of upstream ORFs in eukaryotes. Trends Biochem. Sci. *44*, 782–794. https://doi.org/10.1016/j.tibs.2019.03.002.
15. Tanaka, M., Sotta, N., Yamazumi, Y., Yamashita, Y., Miwa, K., Murota, K., Chiba, Y., Hirai, M.Y., Akiyama, T., Onouchi, H., et al. (2016). The minimum open reading frame, AUG-stop, induces boron-dependent ribosome stalling and mRNA degradation. Plant Cell *28*, 2830–2849. https://doi.org/10.1105/tpc.16.00481.
16. Ingolia, N.T., Ghaemmaghami, S., Newman, J.R.S., and Weissman, J.S. (2009). Genome-wide analysis in vivo of translation with nucleotide resolution using ribosome profiling. Science *324*, 218–223. https://doi.org/10.1126/science.1168978.
17. Chothani, S.P., Adami, E., Widjaja, A.A., Langley, S.R., Viswanathan, S., Pua, C.J., Zhihao, N.T., Harmston, N., D'Agostino, G., Whiffin, N., et al. (2022). A high-resolution map of human RNA translation. Mol. Cell *82*, 2885–2899.e8. https://doi.org/10.1016/j.molcel.2022.06.023.
18. Zheng, B., Larkin, D.W., Albrecht, U., Sun, Z.S., Sage, M., Eichele, G., Lee, C.C., and Bradley, A. (1999). The mPer2 gene encodes a functional component of the mammalian circadian clock. Nature *400*, 169–173. https://doi.org/10.1038/22118.
19. Lee, C., Etchegaray, J.P., Cagampang, F.R., Loudon, A.S., and Reppert, S.M. (2001). Posttranslational mechanisms regulate the mammalian circadian clock. Cell *107*, 855–867. https://doi.org/10.1016/s0092-8674(01)00610-9.
20. Zheng, B., Albrecht, U., Kaasik, K., Sage, M., Lu, W., Vaishnav, S., Li, Q., Sun, Z.S., Eichele, G., Bradley, A., and Lee, C.C. (2001). Nonredundant roles of the mPer1 and mPer2 genes in the mammalian circadian clock. Cell *105*, 683–694.
21. Doi, M., Shimatani, H., Atobe, Y., Murai, I., Hayashi, H., Takahashi, Y., Fustin, J.M., Yamaguchi, Y., Kiyonari, H., Koike, N., et al. (2019). Non-coding cis-element of Period2 is essential for maintaining organismal circadian behaviour and body temperature rhythmicity. Nat. Commun. *10*, 2563. https://doi.org/10.1038/s41467-019-10532-2.
22. Tainaka, M., Doi, M., Inoue, Y., Murai, I., and Okamura, H. (2018). Circadian PER2 protein oscillations do not persist in cycloheximide-treated

mouse embryonic fibroblasts in culture. Chronobiol. Int. *35*, 132–136. https://doi.org/10.1080/07420528.2017.1316731.

23. Tamaru, T., Hattori, M., Honda, K., Benjamin, I., Ozawa, T., and Takamatsu, K. (2011). Synchronization of circadian Per2 rhythms and HSF1-BMAL1:CLOCK interaction in mouse fibroblasts after short-term heat shock pulse. PLoS One *6*, e24521. https://doi.org/10.1371/journal.pone.0024521.

24. Koyanagi, S., Hamdan, A.M., Horiguchi, M., Kusunose, N., Okamoto, A., Matsunaga, N., and Ohdo, S. (2011). cAMP-response element (CRE)-mediated transcription by activating transcription factor-4 (ATF4) is essential for circadian expression of the Period2 gene. J. Biol. Chem. *286*, 32416–32423. https://doi.org/10.1074/jbc.M111.258970.

25. Gerber, A., Esnault, C., Aubert, G., Treisman, R., Pralong, F., and Schibler, U. (2013). Blood-borne circadian signal stimulates daily oscillations in actin dynamics and SRF activity. Cell *152*, 492–503. https://doi.org/10.1016/j.cell.2012.12.027.

26. Tisi, L.C., White, P.J., Squirrell, D.J., Murphy, M.J., Lowe, C.R., and Murray, J.A.H. (2002). Development of a thermostable firefly luciferase. Anal. Chim. Acta *457*, 115–123. https://doi.org/10.1016/s0003-2670(01)01496-9.

27. Lin, R.Z., Hu, Z.W., Chin, J.H., and Hoffman, B.B. (1997). Heat shock activates c-Src tyrosine kinases and phosphatidylinositol 3-kinase in NIH3T3 fibroblasts. J. Biol. Chem. *272*, 31196–31202. https://doi.org/10.1074/jbc.272.49.31196.

28. Sato, S., Fujita, N., and Tsuruo, T. (2000). Modulation of Akt kinase activity by binding to Hsp90. Proc. Natl. Acad. Sci. USA *97*, 10832–10837. https://doi.org/10.1073/pnas.170276797.

29. Yoshihara, T., Naito, H., Kakigi, R., Ichinoseki-Sekine, N., Ogura, Y., Sugiura, T., and Katamoto, S. (2013). Heat stress activates the Akt/mTOR signalling pathway in rat skeletal muscle. Acta Physiol. *207*, 416–426. https://doi.org/10.1111/apha.12040.

30. Kitani, S., Teshima, R., Morita, Y., Ito, K., Matsuda, Y., and Nonomura, Y. (1992). Inhibition of IgE-mediated histamine release by myosin light chain kinase inhibitors. Biochem. Biophys. Res. Commun. *183*, 48–54. https://doi.org/10.1016/0006-291x(92)91607-r.

31. Hausdorff, S.F., Fingar, D.C., Morioka, K., Garza, L.A., Whiteman, E.L., Summers, S.A., and Birnbaum, M.J. (1999). Identification of wortmannin-sensitive targets in 3T3-L1 adipocytes. Dissociation of insulin-stimulated glucose uptake and glut4 translocation. J. Biol. Chem. *274*, 24677–24684. https://doi.org/10.1074/jbc.274.35.24677.

32. Hennessy, B.T., Smith, D.L., Ram, P.T., Lu, Y., and Mills, G.B. (2005). Exploiting the PI3K/AKT pathway for cancer drug discovery. Nat. Rev. Drug Discov. *4*, 988–1004. https://doi.org/10.1038/nrd1902.

33. Crosby, P., Hamnett, R., Putker, M., Hoyle, N.P., Reed, M., Karam, C.J., Maywood, E.S., Stangherlin, A., Chesham, J.E., Hayter, E.A., et al. (2019). Insulin/IGF-1 drives PERIOD synthesis to entrain circadian rhythms with feeding time. Cell *177*, 896–909.e20. https://doi.org/10.1016/j.cell.2019.02.017.

34. Zhou, J., Wan, J., Gao, X., Zhang, X., Jaffrey, S.R., and Qian, S.B. (2015). Dynamic m(6)A mRNA methylation directs translational control of heat shock response. Nature *526*, 591–594. https://doi.org/10.1038/nature15377.

35. Fustin, J.M., Doi, M., Yamaguchi, Y., Hida, H., Nishimura, S., Yoshida, M., Isagawa, T., Morioka, M.S., Kakeya, H., Manabe, I., and Okamura, H. (2013). RNA-methylation-dependent RNA processing controls the speed of the circadian clock. Cell *155*, 793–806. https://doi.org/10.1016/j.cell.2013.10.026.

36. Hirota, T., Lee, J.W., Lewis, W.G., Zhang, E.E., Breton, G., Liu, X., Garcia, M., Peters, E.C., Etchegaray, J.P., Traver, D., et al. (2010). High-throughput chemical screen identifies a novel potent modulator of cellular circadian rhythms and reveals CKIalpha as a clock regulatory kinase. PLoS Biol. *8*, e1000559. https://doi.org/10.1371/journal.pbio.1000559.

37. Narasimamurthy, R., Hunt, S.R., Lu, Y., Fustin, J.M., Okamura, H., Partch, C.L., Forger, D.B., Kim, J.K., and Virshup, D.M. (2018). CK1delta/epsilon protein kinase primes the PER2 circadian phosphoswitch. Proc. Natl. Acad. Sci. USA *115*, 5986–5991. https://doi.org/10.1073/pnas.1721076115.

38. Goda, T., Doi, M., Umezaki, Y., Murai, I., Shimatani, H., Chu, M.L., Nguyen, V.H., Okamura, H., and Hamada, F.N. (2018). Calcitonin receptors are ancient modulators for rhythms of preferential temperature in insects and body temperature in mammals. Genes Dev. *32*, 140–155. https://doi.org/10.1101/gad.307884.117.

39. Gotic, I., Omidi, S., Fleury-Olela, F., Molina, N., Naef, F., and Schibler, U. (2016). Temperature regulates splicing efficiency of the cold-inducible RNA-binding protein gene Cirbp. Genes Dev. *30*, 2005–2017. https://doi.org/10.1101/gad.287094.116.

40. Spörl, F., Schellenberg, K., Blatt, T., Wenck, H., Wittern, K.P., Schrader, A., and Kramer, A. (2011). A circadian clock in HaCaT keratinocytes. J. Invest. Dermatol. *131*, 338–348. https://doi.org/10.1038/jid.2010.315.

41. Hoyle, N.P., Seinkmane, E., Putker, M., Feeney, K.A., Krogager, T.P., Chesham, J.E., Bray, L.K., Thomas, J.M., Dunn, K., Blaikley, J., and O'Neill, J.S. (2017). Circadian actin dynamics drive rhythmic fibroblast mobilization during wound healing. Sci. Transl. Med. *9*, eaal2774. https://doi.org/10.1126/scitranslmed.aal2774.

42. Cao, R., Gkogkas, C.G., de Zavalia, N., Blum, I.D., Yanagiya, A., Tsukumo, Y., Xu, H., Lee, C., Storch, K.F., Liu, A.C., et al. (2015). Light-regulated translational control of circadian behavior by eIF4E phosphorylation. Nat. Neurosci. *18*, 855–862. https://doi.org/10.1038/nn.4010.

43. Cao, R., Robinson, B., Xu, H., Gkogkas, C., Khoutorsky, A., Alain, T., Yanagiya, A., Nevarko, T., Liu, A.C., Amir, S., and Sonenberg, N. (2013). Translational control of entrainment and synchrony of the suprachiasmatic circadian clock by mTOR/4E-BP1 signaling. Neuron *79*, 712–724. https://doi.org/10.1016/j.neuron.2013.06.026.

44. Bohlen, J., Harbrecht, L., Blanco, S., Clemm von Hohenberg, K., Fenzl, K., Kramer, G., Bukau, B., and Teleman, A.A. (2020). DENR promotes translation reinitiation via ribosome recycling to drive expression of oncogenes including ATF4. Nat. Commun. *11*, 4676. https://doi.org/10.1038/s41467-020-18452-2.

45. Park, H.G., Han, S.I., Oh, S.Y., and Kang, H.S. (2005). Cellular responses to mild heat stress. Cell. Mol. Life Sci. *62*, 10–23. https://doi.org/10.1007/s00018-004-4208-7.

46. Murata, N., and Los, D.A. (1997). Membrane fluidity and temperature perception. Plant Physiol. *115*, 875–879. https://doi.org/10.1104/pp.115.3.875.

47. Kowalska, E., Ripperger, J.A., Hoegger, D.C., Bruegger, P., Buch, T., Birchler, T., Mueller, A., Albrecht, U., Contaldo, C., and Brown, S.A. (2013). NONO couples the circadian clock to the cell cycle. Proc. Natl. Acad. Sci. USA *110*, 1592–1599. https://doi.org/10.1073/pnas.1213317110.

48. Dekoninck, S., and Blanpain, C. (2019). Stem cell dynamics, migration and plasticity during wound healing. Nat. Cell Biol. *21*, 18–24. https://doi.org/10.1038/s41556-018-0237-6.

49. Nagoshi, E., Saini, C., Bauer, C., Laroche, T., Naef, F., and Schibler, U. (2004). Circadian gene expression in individual fibroblasts: cell-autonomous and self-sustained oscillators pass time to daughter cells. Cell *119*, 693–705. https://doi.org/10.1016/j.cell.2004.11.015.

50. O'Neill, J.S., and Hastings, M.H. (2008). Increased coherence of circadian rhythms in mature fibroblast cultures. J. Biol. Rhythms *23*, 483–488. https://doi.org/10.1177/0748730408326682.

51. Sun, B.K., Siprashvili, Z., and Khavari, P.A. (2014). Advances in skin grafting and treatment of cutaneous wounds. Science *346*, 941–945. https://doi.org/10.1126/science.1253836.

52. VanInsberghe, M., van den Berg, J., Andersson-Rolf, A., Clevers, H., and van Oudenaarden, A. (2021). Single-cell Ribo-seq reveals cell

cycle-dependent translational pausing. Nature *597*, 561–565. https://doi.org/10.1038/s41586-021-03887-4.

53. Balsalobre, A., Brown, S.A., Marcacci, L., Tronche, F., Kellendonk, C., Reichardt, H.M., Schütz, G., and Schibler, U. (2000). Resetting of circadian time in peripheral tissues by glucocorticoid signaling. Science *289*, 2344–2347. https://doi.org/10.1126/science.289.5488.2344.
54. Le Minh, N., Damiola, F., Tronche, F., Schütz, G., and Schibler, U. (2001). Glucocorticoid hormones inhibit food-induced phase-shifting of peripheral circadian oscillators. EMBO J. *20*, 7128–7136. https://doi.org/10.1093/emboj/20.24.7128.
55. Sato, S., Dyar, K.A., Treebak, J.T., Jepsen, S.L., Ehrlich, A.M., Ashcroft, S.P., Trost, K., Kunzke, T., Prade, V.M., Small, L., et al. (2022). Atlas of exercise metabolism reveals time-dependent signatures of metabolic homeostasis. Cell Metab. *34*, 329–345.e8. https://doi.org/10.1016/j.cmet.2021.12.016.
56. Asher, G., Reinke, H., Altmeyer, M., Gutierrez-Arcelus, M., Hottiger, M.O., and Schibler, U. (2010). Poly(ADP-ribose) polymerase 1 participates in the phase entrainment of circadian clocks to feeding. Cell *142*, 943–953. https://doi.org/10.1016/j.cell.2010.08.016.
57. Acosta-Rodríguez, V., Rijo-Ferreira, F., Izumo, M., Xu, P., Wight-Carter, M., Green, C.B., and Takahashi, J.S. (2022). Circadian alignment of early onset caloric restriction promotes longevity in male C57BL/6J mice. Science *376*, 1192–1202. https://doi.org/10.1126/science.abk0297.
58. Grimm, D., Lee, J.S., Wang, L., Desai, T., Akache, B., Storm, T.A., and Kay, M.A. (2008). In vitro and in vivo gene therapy vector evolution via multispecies interbreeding and retargeting of adeno-associated viruses. J. Virol. *82*, 5887–5911. https://doi.org/10.1128/JVI.00254-08.
59. Yamaguchi, Y., Murai, I., Goto, K., Doi, S., Zhou, H., Setsu, G., Shimatani, H., Okamura, H., Miyake, T., and Doi, M. (2021). Gpr19 is a circadian clock-controlled orphan GPCR with a role in modulating free-running period and light resetting capacity of the circadian clock. Sci. Rep. *11*, 22406. https://doi.org/10.1038/s41598-021-01764-8.
60. Seluanov, A., Vaidya, A., and Gorbunova, V. (2010). Establishing primary adult fibroblast cultures from rodents. J. Vis. Exp. *44*, e2033. https://doi.org/10.3791/2033.
61. Mito, M., Mishima, Y., and Iwasaki, S. (2020). Protocol for disome profiling to survey ribosome collision in humans and zebrafish. STAR Protoc. *1*, 100168. https://doi.org/10.1016/j.xpro.2020.100168.
62. Sasaki, L., Hamada, Y., Yarimizu, D., Suzuki, T., Nakamura, H., Shimada, A., Pham, K.T.N., Shao, X., Yamamura, K., Inatomi, T., et al. (2022). Intracrine activity involving NAD-dependent circadian steroidogenic activity governs age-associated meibomian gland dysfunction. Nat. Aging *2*, 105–114.
63. Morioka, S., Nakanishi, H., Yamamoto, T., Hasegawa, J., Tokuda, E., Hikita, T., Sakihara, T., Kugii, Y., Oneyama, C., Yamazaki, M., et al. (2022). A mass spectrometric method for in-depth profiling of phosphoinositide regioisomers and their disease-associated regulation. Nat. Commun. *13*, 83. https://doi.org/10.1038/s41467-021-27648-z.

STAR★METHODS

KEY RESOURCES TABLE

REAGENT or RESOURCE	SOURCE	IDENTIFIER
Antibodies		
anti-Per2	Doi et al., 2019[21]	N/A
anti-Cry2	MBL	PM082
anti-Clock	MBL	D349-3
anti-Bmal1	MBL	D335-3
anti-HSF1	Abcam	Cat# Ab61382; RRID: AB_942016
anti-p-CREB	Cell Signaling	Cat# 9198; RRID: AB_2561044
anti-FosB	Cell Signaling	Cat# 2251; RRID: AB_2106903
anti-tubulin	Sigma	Cat# T6199; RRID: AB_477583
anti-β-actin	Sigma	Cat# A5441; RRID: AB_476744
Bacterial and virus strains		
AAV-DJ	Grimm et al., 2008[58]	N/A
DH5α *Escherichia coli*	Takara Bio	#9057
Chemicals, peptides, and recombinant proteins		
17β-hydroxy-wortmannin	Cayman	#13812
PI3-Kinase α Inhibitor 2	Cayman	#21197
GSK1059615	Cayman	#11569
EGF	Peprotech	14321-54
Dexamethasone	Sigma	D8893
Cycloheximide	Nacalai Tesque	06741-91
Biotin-PEG4-alkyne	Sigma	#764213
KNK437	Sigma	SML0964
Rapamycin	Cayman	#13346
MK2206	Selleck chemicals	S1078
U0126	Cayman	#70970
DZnepA	Sigma	SML0305
Ruthenium Red	Wako	189-03181
Critical commercial assays		
Click-iT Protein Reaction Buffer Kit	Thermo Fisher	C10276
Deposited data		
Ribo-seq and RNA-seq data (for Figures 1, 3, and S1)	This paper	GEO: GSE188529
Ribo-seq data (for Figures 3 and S1)	This paper	GEO: GSE211532
Unprocessed original immunoblot data (for Figures 2, 3, 4, and S2–S6)	This paper	Mendeley Data: https://doi.org/10.17632/k4wygddpkd.1
Experimental models: Cell lines		
Per2::LucTS knock-in MEFs	This paper	N/A
Tet-On 3G NIH3T3	Clontech	#631197; RRID: CVCL_V360
Experimental models: Organisms/strains		
Per2 minimal uORF mutant mice	This paper	RIKEN BRC No. 11461
Oligonucleotides		
Quantitative RT-PCR forward primer for *Per2*: 5′-CTC ACT GAG ATT CGG GAT ATG-3′	Doi et al., 2019[21]	N/A
Quantitative RT-PCR reverse primer for *Per2*: 5′-CTC CCA CCT TGT CTC CAG TC-3′	Doi et al., 2019[21]	N/A
Quantitative RT-PCR forward primer for *Cirp*: 5′-GCA GAT CTC CGA AGT GGT G-3′	Morf et al., 2012[8]	N/A

(*Continued on next page*)

Continued

REAGENT or RESOURCE	SOURCE	IDENTIFIER
Quantitative RT-PCR reverse primer for *Cirp*: 5′-CAG CCT GGT CAA CTC TGA T-3′	Morf et al., 2012[8]	N/A
Quantitative RT-PCR forward primer for *Rplp0*: 5′-CTC ACT GAG ATT CGG GAT ATG-3′	Doi et al., 2019[21]	N/A
Quantitative RT-PCR reverse primer for *Rplp0*: 5′-CTC CCA CCT TGT CTC CAG TC-3′	Doi et al., 2019[21]	N/A
Probes and primers for Taqman qPCR, see Table S2	Doi et al., 2019,[21] Yamaguchi et al., 2021[59]	N/A
shRNA targeting sequence for control: 5′-ATA ACA TGG CCA TCA TCA AGG AGT TCA TG-3′	This paper	N/A
shRNA targeting sequence for *Cirp* #1: 5′-CAG AGA CAG CTA TGA CAG TTA-3′	Thermo Fisher	https://www.thermofisher.com/jp/ja/home/life-science/rnai/synthetic-rnai-analysis.html
shRNA targeting sequence for *Cirp* #2: 5′-CGT CCT TCC ATG GCT GTA ATT-3′	Thermo Fisher	https://www.thermofisher.com/jp/ja/home/life-science/rnai/synthetic-rnai-analysis.html
Recombinant DNA		
pHSE-Luc	Clontech	#K2049-1
pCRE-Luc	Clontech	#K2049-1
pSRE-Luc	Clontech	#K2049-1
pTRE3G-Luc	Clontech	#631168
Software and algorithms		
STAR v2.7.0	N/A	https://github.com/alexdobin/STAR
Samtools v1.10	N/A	https://github.com/samptools/samtools
fp-framing, fp-transcript	N/A	https://github.com/ingolia-lab/RiboSeq
ImageJ	NIH	https://imagej.nih.gov/ij/
Prism 8	GraphPad	N/A

RESOURCE AVAILABILITY

Lead contact

Further information and requests for resources and reagents should be directed to and will be fulfilled by the lead contact, Masao Doi (doimasao@pharm.kyoto-u.ac.jp).

Materials availability

Per2 m-uORF mutant mouse line has been deposited to RIKEN BioResource Research Center (RIKEN BRC No. 11461, https://knowledge.brc.riken.jp/resource/animal/). All other reagents generated in this study are available from the lead contact with a completed materials transfer agreement.

Data and code availability

- Ribo-seq and RNA-seq data have been deposited at GEO and are publicly available as of the date of publication. Accession numbers are GSE188529 and GSE211532. Unprocessed original immunoblot data have been deposited to Mendely Data are available at: https://doi.org/10.17632/k4wygddpkd.1. All other data reported in this paper will be shared by the lead contact upon request.
- This paper does not report original code.
- Any additional information required to reanalyze the data reported in this paper is available from the lead contact upon request.

EXPERIMENTAL MODEL AND SUBJECT DETAILS

Cell lines

The Tet-On 3G NIH3T3 cell line was purchased from Clontech (Mountain View, CA) and maintained in Dulbecco's modified Eagle's medium (DMEM) supplemented with 10% fetal bovine serum (FBS), 100 μg/mL G418 at 37°C in a humidified 5% CO_2 atmosphere. To generate Per2::LucTS knockin MEF cells, we used a firefly luciferase containing the mutations T214A, I232A, F295L, and E354K (*LucTS*).[26] The *LucTS* coding sequence was inserted in frame before the endogenous stop codon of *Per2* using CRISPR/Cas9

technology. The gRNA sequence used was 5′-TGA GGT ATC ACA GAT TCC CG-3′. The edited genome sequence was verified by PCR-Sanger sequencing. Cells were maintained in DMEM/Ham's F-12 (1:1) supplemented with 10% FBS.

Mice

The C57BL/6J male mice 6–8 weeks old were purchased from Japan SLC (Shizuoka, Japan). *Per2* m-uORF mutant mice were established at the Animal Resource Center for Infectious Diseases, Research Institute for Microbial Diseases, Osaka University, by CRISPR/Cas9-based genome editing using C57BL/6J mouse zygotes. The sequences of gRNA and the template oligonucleotide were 5′-TTT CCA CTA TGT GAC AGC GGA GG-3′ and 5′-CAA TGG CGC GCG CAG GGG CGG GCT CAG CGC GCG CGG TCA CGT TTT CCA CTT AAC AGC GGA GGG CGA CGC GGC GGC AGC GGC GCT ACT GGG ACT AGC GGC TCC G-3′, respectively. The edited sequence was verified by Sanger DNA sequencing. All procedures for animal experiments in this study were conducted in compliance with the Ethical Regulations of Kyoto University and performed under protocols approved by the Animal Care and Experimentation Committee of Kyoto University and the Institutional Animal Care and Use Committees of Osaka university.

Primary fibroblasts

Primary fibroblasts were isolated from the lung or skin of adult *Per2* m-uORF mutant mice and control wild-type siblings, according to a protocol previously established.[60] Briefly, the tissue fragments were cut into ~1 mm pieces and incubated in Blendzyme 3 (0.14 Wunsch units/mL, Roche, 11814176001)-containing DMEM/F12 medium at 37°C for 90 min. After centrifugation for 5 min × 524 *g*, the pellet was resuspended in DMEM/F12 media supplemented with 15% FBS, and then incubated at 37°C, 5% CO_2. Cells used for experiments were between passages 2 and 4.

METHOD DETAILS

Temperature control

WTS was applied to cells by transferring the cell dish from a 35°C incubator to a 38.5°C-prewarmed incubator. The temperature of the medium was measured using an electronic thermometer and verified to approach 38.5 °C at 7–8 min after being transferred. Application of simulated body temperature was performed using a custom-modified convection-ventilated incubator box, in which the temperature was controlled by a Peltier device and forced air circulation. This device enabled the programming and recording of temperature profiles in real time with an accuracy of 0.1°C.

Ribo-seq and RNA-seq analysis

We used Dex-synchronized MEF cells treated with or without WTS for 2 h. Cells were lysed with a buffer containing 20 mM Tris-HCl [pH 7.5], 150 mM NaCl, 5 mM $MgCl_2$, 1 mM DTT, 1% Triton X-100, and 100 μg/mL cycloheximide (CHX). Following the digestion of genomic DNA with DNase I (~25 U/mL, Thermo Fisher Scientific), lysates were centrifuged at 20,000 × *g* and the resultant supernatant was processed for library generation.[61] For Ribo-seq, samples (10 μg RNA each) were digested with 20 U RNase (Epicentre) at 25°C for 45 min, and the RNA fragments protected by ribosomes ranging 17–34 nt were gel-excised and ligated with linker oligonucleotides followed by rRNA depletion using Ribo-Zero Gold rRNA Removal Kit (Illumina). The resultant RNA fragments were reverse transcribed with Photoscript II (NEB) and circularized using CircLigaseII (Epicentre). The circularized cDNA templates were PCR amplified for 6 to 8 cycles using Phusion polymerase (NEB) and sequenced on an Illumina Hiseq X or HiSeq 4000 instrument. For RNA-seq, samples were subjected to library construction using TruSeq Stranded Total RNA Gold (Illumina) and sequenced on HiSeq 4000 as described[62]; single-end reads (150 bp for experiment 1 and 50 bp for the others) were mapped to the mouse genome (GRCm38/mm10) using STAR (version 2.7.0) and sorted and indexed using samtools (version 1.10). For filtering rRNA and tRNA, STAR was used with rRNA and tRNA annotations downloaded from the UCSC table browser. Footprints ranging from 20–34 nt were used for further analysis. In Figure 3G, the minimal uORF was identified as NUG-stop (N = A, C, U or G). The A-site location of the Ribo-seq footprints and 3-nucleotide periodicity, which is supplied to validate our Ribo-seq data quality (Table S1), were calculated as described[61] using the fp-transcript and fp-framing, respectively (https://github.com/ingolia-lab/RiboSeq).

Polysome profiling

Linear 15%–50% sucrose gradients were prepared using a BioComp Gradient Master (Biocomp Instruments). Sucrose was dissolved in 20 mM Tris-HCl [pH 7.5], 10 mM $MgCl_2$, 100 mM KCl, 2 mM DTT, 100 U/mL human recombinant RNase Inhibitor (TOYOBO), and 100 μg/mL CHX. Cells were lysed in ice-cold buffer containing 20 mM Tris-HCl [pH 7.5], 150 mM NaCl, 5 mM $MgCl_2$, 1 mM DTT, 1% Triton X-100, and 100 μg/mL CHX. Following the digestion of genomic DNA with DNase I (~25 U/mL, Thermo Fisher Scientific), lysates were centrifuged at 20,000 × *g*. The supernatants were loaded on top of the gradients and sedimented at 35,000 rpm in an SW41 rotor at 4°C for 2 h. After centrifugation, gradients were fractionated using the Gradient Master instrument with continuous monitoring at A260. RNA in each fraction was extracted using TRIzol LS reagent (Thermo Fisher Scientific).

Immunoblotting

To minimize proteolysis of the endogenous Per2 protein, cells and tissues (dorsal ear skin and lung) were lysed immediately in Laemmli buffer containing 1x cOmplete Protease Inhibitor cocktail (Roche Diagnostics), as described previously.[21] Immunoblots

were performed using our standard method with affinity-purified anti-mPer2 rabbit polyclonal antibody (final concentration, 2 μg/mL)[21] or commercially available antibodies against α-Tubulin (Sigma Aldrich, T6199, 1:1,000), β-actin (Sigma Aldrich, A5441, 1:1,000), Clock (MBL, D349-3, 1:1,200), Bmal1 (MBL, D335-3, 1:200), Cry2 (MBL, PM082, 1:200), HSF1 (abcam, ab61382, 1:200), p-CREB (Cell Signaling, #9198, 1:1,000), and FosB (Cell Signaling, #2251, 1:1,000). The CHX chase assay was performed by adding CHX (100 μg/mL) to the medium at Time 24. Where specified, cells were treated with 17β-hydroxy Wortmannin (Cayman chemical, 10 μM), PI3-Kinase α Inhibitor 2 (Cayman chemical, 10 μM), GSK1059615 (Cayman chemical 10 μM), or EGF (Peprotech, 10 ng/mL).

Labeling of de novo protein synthesis

Dex-synchronized cells were preincubated with a Met/Cys-free DMEM medium (Thermo Fisher Scientific) for 3 h before experiments. [^{35}S]Methionine (14.8 MBq/sample, Muromachi Kikai) was added to the medium at Time 0 and incubated for 2 h with or without WTS. Cells were lysed in RIPA buffer (50 mM Tris-HCl [pH 8.0], 150 mM NaCl, 0.1% SDS, 1% Nonidet P40, 1% sodium deoxycholate) containing 1x cOmplete Protease Inhibitor cocktail (Roche Diagnostics) and subjected to immunoprecipitation with anti-mPer2 polyclonal antibody[21] or anti-Cry2 antibody (MBL, PM082). The immunoprecipitate was separated by SDS-PAGE and visualized with an X-ray film (Kodak). For click-labeling experiments, azidohomoalanine (AHA) was added to the medium at Time 0 (final concentration, 50 μM) instead of [^{35}S]Methionine. Cells were lysed in RIPA buffer containing 1x cOmplete Protease Inhibitor cocktail. The lysates were conjugated with biotin-PEG4-alkyne (Sigma Aldrich) using the Click-iT Protein Reaction Buffer Kit (Thermo Fisher Scientific). After removal of excess free biotin-PEG4-alkyne using PD SpinTrap G-25 columns (Cytiva), AHA-biotin-alkyne labeled proteins were affinity-purified with streptavidin beads (Thermo Fisher Scientific). The precipitates were analyzed by immunoblotting using the anti-mPer2 polyclonal antibody,[21] anti-Cry2 (MBL, PM082), or anti-β-actin antibodies (Sigma Aldrich, A5441). Biotin-labeled proteins were detected using Vectastain Elite ABC Standard Kit (Vector Laboratories).

LucTS reporter assay

pHSE-LucTS, pCRE-LucTS, and pSRE-LucTS were generated by replacing the Luc coding sequence of pHSE-Luc, pCRE-Luc, and pSRE-Luc (all vectors from Clontech) with the LucTS. One day after transfection, MEFs were either treated with WTS, heat shock (42°C), 100 μM forskolin, or 50% bovine serum. The mean values of the 4 h pre-stimulation baseline of lumi-nescence of pHSE-, pCRE-, and pSRE-LucTS were set to 1. The Tet-inducible expression vector pTRE3G (Clontech) was used to construct the *Per2* 5′ UTR-LucTS vectors. The 5′ UTR region of the pTRE3G vector was substituted with the full-length *Per2* 5′ UTR sequence of mouse (NM_011066) or human (XM_006712824) origin. Mutagenesis of the *Per2* m-uORF was performed using a standard sequential PCR method.[21] Tet-On 3G NIH3T3cells were transfected with a plasmid using the Viofectin reagent (Viogene). To reduce technical variation between transfections, the transfection was performed in a single dish and the cells were split into test dishes. D-luciferin (Promega) was added to the medium before experiments.[21] Cells were treated with doxycycline (1 μg/mL). Luminescence was continuously monitored using a custom-modified dish-type luminometer AB-2550 Kronos Dio (ATTO), which enables the programming and recording of temperature profiles in real-time with an accuracy of 0.1°C. Luminescence was measured for 2 min at 30-min intervals. Values were normalized to the luminescence intensity that was recorded 30 min before WTS. The fold increase was calculated by dividing the intensity of WTS-treated cells by that of non-treated controls.

Per2::LucTS cell-based kinase inhibitor assay

Per2::LucTS cells were treated with a compound in the Kinase Screening Library (Cayman Chemical, #10505) at a concentration of 10 μM/0.1% DMSO immediately before WTS. The score was calculated using the following formula;

$$Score = -log_2 \frac{Td\ of\ tested\ compound}{Td\ of\ vehicle}$$

where *Td* represents the difference in the half-maximum time between WTS and no-WTS cells. The results of compounds that profoundly affect basal LucTS activity were omitted. To evaluate dose dependency, Wortm was administrated at a concentration of 0.3, 1, 10, 30, 100, and 1000 nM. Where indicated, KNK437 (Sigma Aldrich, 100 μM), Rapamycin (Cayman chemical, 20 nM), MK2206 (Selleck chemicals, 10 μM), U0126 (Cayman chemical, 10 μM), DZnepA (Sigma Aldrich, 100 μM), D4476 (Cayman chemical, 5 μM), and Ruthenium Red (Wako, 10 μM) were used.

Quantification of PIP_3 species

Cells were incubated in a serum-free medium 1 day before experiments and sampled after 2 h of WTS. PIP_3 was measured using an LC system [UltiMate 3000 (Thermo Fisher Scientific) and HTC PAL autosampler (CTC Analytics)] connected to a triple-stage quadrupole mass spectrometer (TSQ Vantage, Thermo Fisher), as described previously.[63] Briefly, the samples were mixed with internal standards, purified with DEAE Sepharose Fast Flow (10% slurry), and methylated using trimethylsilyl diazomethane. Methylated lipids were then separated on a C18 column (GL Sciences) using a solvent gradient as follows: 0–1 min hold 70% A/30% B, 1–3 min constant gradient to reach 90% A/10% B, 3–7.5 min constant at 90% A/10% B, 7.5–13 min 30% A/70% B, where mobile phase A was acetonitrile/water/70% ethylamine (800:200:1.3) and mobile phase B was acetonitrile/isopropanol/70% ethylamine (200:800:1.3). Multiple reaction monitoring (MRM) was employed in positive ion mode. Values were normalized using the sum of the phosphatidylinositol (PI) values.

Quantitative RT-PCR

Total cell RNA was extracted using FastGene RNA basic kit (Nippon Genetics). cDNA was synthesized using SuperScript VILO cDNA synthesis kit (Invitrogen) and quantitative real-time PCR was performed using THUNDERBIRD SYBR qPCR mix (TOYOBO) and StepOnePlus (Applied Biosystems). *Rplp0* was used as an internal control. The primer sets used in this study included: *Rplp0*, Fw: 5′-CTC ACT GAG ATT CGG GAT ATG-3′, Rv: 5′-CTC CCA CCT TGT CTC CAG TC-3′, *Per2*, 5′-CTC ACT GAG ATT CGG GAT ATG-3′, Rv: 5′-CTC CCA CCT TGT CTC CAG TC-3′, and *Cirp*, Fw: 5′-GCA GAT CTC CGA AGT GGT G-3′, Rv: 5′-CAG CCT GGT CAA CTC TGA T-3′. To quantify *Per2* mRNA levels in the nucleus and cytosol, cellular fractionation was performed as described previously.[35] Briefly, cells were transferred to a precooled 1.5 mL tube and cell walls were disrupted using 10 passages with a 25G needle, on ice. Cells were centrifuged at 700 × *g* for 10 min at 4°C, the supernatant (containing cytoplasmic RNA) carefully removed and transferred to a new tube on ice. The pellet was resuspended and layered on top of a 24% sucrose cushion. Nuclei were then centrifuged at 20,000 × *g* for 10 min at 4°C. The supernatant was discarded, and nuclei were homogenized in 1 mL Sepasol-RNA I Super G (Nacalai Tesque) by full-speed vortexing, then incubated at 65°C, vortexing frequently until fully homogenized. A customized panel of 17 clock and clock-controlled genes were analyzed using a BioMark HD System (Fluidigm) with a 48.48 Fluidigm BioMark Dynamic Array chip (Fluidigm). TaqMan probe and primer sets were shown in Table S2.[21,59]

AAV-mediated gene knockdown

Aliquots of the AAV harboring hU6-shRNAs were added to the cultured media and cells were incubated for 7 days to achieve sufficient gene knockdown. The target sequence of shRNA used in this study included: mCherry shRNA (control), 5′-ATA ACA TGG CCA TCA TCA AGG AGT TCA TG-3′, *Cirp* shRNA #1 5′-CAG AGA CAG CTA TGA CAG TTA-3′, and *Cirp* shRNA #2, 5′-CGT CCT TCC ATG GCT GTA ATT-3′. AAV-shRNA with a mutant form of the AAV-2 cap gene (AAV-DJ)[58] was produced using a triple-transfection, helper-free method. The titer of shRNA vectors were (genome copies/mL): control shRNA, 1.9×10^{11}, *Cirp* shRNA #1, 1.4×10^{11}, *Cirp* shRNA #2, 1.0×10^{11}. The knockdown efficiency of *Cirp* was analyzed using real-time quantitative PCR analysis.

In vitro and *in vivo* wound assay

For the *in vitro* scratch wound assay, the confluent monolayer of culture was scratched with a sterile 200 μL pipette tip to create a scratch wound. For the *in vivo* wound healing assay, age-matched male mice (9–11 weeks old) were anesthetized, shaved and subjected to two bilateral full-thickness 4-mm circular biopsy punches to the dorsal skin. The wound site was digitally photographed at the indicated time points.

Locomotor activity recording

Adult male mice (8–12 weeks old) were housed individually in light-tight, ventilated closets under indicated lighting conditions with ad libitum access to food and water. Locomotor activity was recorded via passive infrared sensors (PIRs, FA-05F5B; Omron) with 1-min resolution and analyzed with CLOCKLAB software (Actimetrics). Free-running period in DD was determined with χ^2 periodogram.

High fat diet feeding

At 4 weeks of age, animals were placed on a standard chow diet (3.59 kcal/g, Oriental Yeast, MF) or a HFD (5.23 kcal/g, 60% kcal from fat, Research Diets, D12492) for 20 weeks. Body weight was measured weekly. Food intake was measured for a week at the age of 16 weeks.

QUANTIFICATION AND STATISTICAL ANALYSIS

Western blot band intensities and the area of wounds were quantified using Image J software. Statistical analyses and plots were generated with GraphPad Prism 8, using the statistical tests indicated in the figure legends. For circular statistics, Rayleigh's uniformity test was performed using Oriana 4 software (Kovacs Computer Services).